Title
Constraining early to middle Eocene climate evolution of the southwest Pacific and Southern Ocean

Authors
Dallanave, Edoardo
Bachtadse, Valerian
Crouch, Erica M
et al.

Publication Date
2016

DOI
10.1016/j.epsl.2015.11.010

Peer reviewed

CONSTRAINING EARLY TO MIDDLE EOCENE CLIMATE EVOLUTION OF THE SOUTHWEST PACIFIC AND SOUTHERN OCEAN.

Edoardo Dallanave*[,1], Valerian Bachtadse[1], Erica M. Crouch[3], Lisa Tauxe[2], Claire L. Shepherd[3,4], Hugh E.G. Morgans[3], Christopher J. Hollis[3], Benjamin R. Hines[3,4], Saiko Sugisaki[2].

*Corresponding author; email: dallanave@geophysik.uni-muenchen.de. Phone: +49 (0) 89 2180 4206. Fax: +49 (0) 89 2180 4205.

[1]Department of Earth and Environmental Science, Ludwig-Maximilians University, Munich D-80333, Germany.

[2]Scripps Institution of Oceanography, UCSD, 9500 Gilman Drive, La Jolla, California 92093–0220, USA

[3]GNS Science, PO Box 30368, Lower Hutt 5040, New Zealand

[4] School of Geography, Environment and Earth Sciences, Victoria University of Wellington, PO Box 600, Wellington 6140, New Zealand

Abstract

One of the major deficiencies of the global database for the early Paleogene is the scarcity of reliable magnetostratigraphically-calibrated climate records from the southern Pacific Ocean, the largest ocean basin during this time. We present a new magnetostratigraphic record from marine sediments cropping out along the mid-Waipara River, South Island, New Zealand. Fully oriented samples for paleomagnetic analyses were collected along 45 m of stratigraphic section, which encompasses magnetic polarity Chrons from C23n to C21n. These results are integrated with foraminiferal, calcareous nannofossil, and dinoflagellate cyst (dinocyst) biostratigraphy from samples collected in three different expeditions along a total of ~80 m of section. Biostratigraphic data indicates continuous sedimentation from the Waipawan to the Heretaungan New Zealand stages (i.e., Ypresian–Lutetian international stages), from about 55.5 to 46 Ma. We provide the first magnetostratigraphically-calibrated age of 48.88 Ma for the base of the New Zealand Heretaungan Stage (latest early Eocene). A reexamination based on

discrete samples of the magnetostratigraphy of Ocean Drilling Program (ODP) Site 1172 (East Tasman Plateau) demonstrates that no reliable magnetic polarity reversals can be determined for the early Eocene part of the core, which has been used as a reference chronology for the Southwest Pacific Ocean. We apply the robust magneto-biochronology from mid-Waipara to aid the correlation of ODP Site 1172 as well as for Integrated Ocean Drilling Program (IODP) Site U1356 (Wilkes Land Margin, Antarctica) with the international time scale by means of dinocyst biostratigraphy. This integrated chronology allows revision of the published TEX_{86} sea surface temperature proxy records from the three localities, significantly improving the age control for the Southwest Pacific and Southern Ocean climate history during the early and middle Eocene

1. Introduction

During the early Eocene, the Earth experienced a long-term global warming event culminating ~52 to 50 Ma in the early Eocene climatic optimum (EECO; e.g., Zachos et al., 2008). The EECO was followed by a cooling trend that continued over the ensuing middle to late Eocene, and ultimately drove the Earth´s climate into a glacial mode with the inception of major Antarctic ice-sheets near the Eocene–Oligocene boundary (Miller et al., 1991; Zachos et al., 2008). In the ice-free world of the early and middle Eocene, the Pacific Ocean played a key role in the heat transport, primarily because of its greater extent relative to the Atlantic Ocean (Huber and Sloan, 2001; Huber and Nof, 2006). Sedimentary records from the South Pacific Ocean are thus particularly important for understanding the evolution of global climate during early Paleogene.

The climate history of the Southwest Pacific and Southern Ocean has become better known in recent years through the application of new paleotemperature proxies, such as the TEX_{86} (TetraEther Index of lipids with 86 carbon atoms) proxy for sea surface temperature (SST), to sedimentary records from Ocean Drilling Program (ODP) Site 1172 in the East Tasman Plateau (Bijl et al., 2009, 2013a), from Integrated Ocean Drilling Program (IODP) Site U1356 on the Wilkes Land Margin, Antarctica (Pross et al., 2012), and from onshore Canterbury Basin, eastern New Zealand, (Burgess et al., 2008; Hollis et al., 2012, 2009; Pancost et al., 2013; Figure 1a, b). SSTs from these three regions indicate that near-tropical conditions (SST of 25–26 °C) extended close to the Antarctic margin during the EECO. This records are however difficult to reconcile with climate models (Huber and Sloan, 2001; Winguth et al., 2010; Huber and Caballero, 2011; Lunt et al., 2012) and with proxies for land temperatures (Pancost et al. 2013) without factoring in seasonal biases and the influences of localized changes in ocean circulation (Hollis et al., 2012).

A point that has tended to be overlooked when comparing these records with those of other regions is that the age control for the New Zealand records has been based entirely on biostratigraphy. Moreover, the magnetostratigraphy that underpins the age models for ODP Site 1172 (Fuller and Touchard, 2004) was based on the intensity of the magnetization rather than on the inclination of the magnetic remanence as usual practice (see Tauxe et al., 2012 for details) and is not reliable, at least for the early Eocene. In the case of IODP Site U1356 the magnetic polarity stratigraphy for the early–middle Eocene is difficult because of very limited (~38%) sediment recovery and some discrepancies between on-board and discrete samples results (Tauxe et al., 2012).

In order to understand the Eocene climate history of the South Pacific and Southern Ocean it is critical to have a robust chronology in which the succession of biotic changes that form the basis of biostratigraphic correlation are tied to the global calibration datums provided by robust magnetostratigraphy. In this paper we present the first early–middle Eocene magnetic polarity stratigraphy, based on fully oriented samples, from the mid-Waipara River section in Canterbury Basin (South Island, New Zealand). During three field campaigns (2003, 2007, and 2012) we have sampled ~45 m of stratigraphic section for paleomagnetism and ~80 m for foraminiferal, calcareous nannofossils, and dinoflagellate cyst (dinocyst) biostratigraphy. Previously published data indicate that the sediments were deposited at upper bathyal depths during the Waipawan–Bortonian New Zealand stages (NZS), i.e. the Ypresian–Lutetian international stages (Morgans et al., 2005; Hollis et al., 2009; Raine et al., 2015). We also re-investigate the early–middle Eocene magnetostratigraphy of ODP Site 1172 by analyzing discrete samples. The magnetic polarity-based correlation of this integrated dataset with the geomagnetic polarity time scale (GPTS) of

Gradstein et al. (2012; GTS12) allows us to improve the chronology of the composite SST proxy records for mid-Waipara, ODP Site 1172 and IODP Site U1356, constraining the timing of the early-middle Eocene climate events in the Southwest Pacific and Southern Ocean.

2. Material and methods

2.1. Mid-Waipara River section

The mid-Waipara River section is located ~13 km west of the Waipara township, northern Canterbury, and includes the area downstream from Doctors Gorge to the top of the Amuri Limestone in the 'lower gorge' (grid reference NZMS 260-M34/755 946 to M34/789 944). The lower and middle Eocene Ashley Mudstone is quite well exposed, with low-dipping calcareous mudstone outcropping along the river bed.

Several different sample collections have been made on the Ashley Mudstone (Morgans et al., 2005). In this paper we discuss three sample suites that have been integrated for the present study. Two sample suites, collected in 2003 and 2007, are logged and integrated into a single composite section (Figure 1c), using a reference marker at the base of the 2003 collection (Morgans et al., 2005). This integrated collection was the focus of several biostratigraphic and geochemical studies, including foraminiferal and dinocyst biostratigraphy, bulk $\delta^{13}C$ isotopes, Mg/Ca ratios, and TEX_{86} analyses (Hollis et al., 2009, 2012; Creech et al., 2010). For our study, samples from the 2007 suite have been examined to improve the foraminiferal, dinocyst and calcareous nannofossil biostratigraphy for the lower part of the section.

In order to complete a magnetostratigraphic study of the lower–middle Eocene sequence at mid-Waipara River, new samples were collected in 2012 from Ashley Mudstone sediments in the same part of the river bed as those collected in 2003. Unfortunately river floods had removed the reference marker and the new collection could not be precisely correlated with the earlier collections. Hence, the 2012 collection has been correlated with the earlier collections by biostratigraphy and lithology (Figure 1c, Table 1). The stratigraphic gap between the base of the 2012 collection (M34/f930) and the top of the 2007 collection (M34/f889) has been inferred from the stratigraphic dip to be ~1 m (Figure 1c).

2.2. Rock- and Paleomagnetism

Paleomagnetic samples were drilled with a gasoline-powered drill and oriented with a magnetic compass. A total of 114 oriented core samples were collected from 80 layers across ~45 stratigraphic meters of Ashley Mudstone, from which we obtained 169 standard ~11 cm^3 oriented specimens for paleomagnetic analyses. A representative set of specimens from the trimmed ends of the core samples was used to investigate the magnetic properties of the sediments by means of isothermal remanent magnetization (IRM) backfield acquisition curves up to 2.4 T. To obtain the median destructive field (MDF) of the specimens, the IRM acquisition was followed by 3-axis AF demagnetization of saturation IRM up to 90 mT. The specimens were then subjected to thermomagnetic curves analysis: they were heated in air up to 650°C in an inducing field of ~800 mT using a variable field translation balance (VFTB; Krása et al., 2007). Curie temperatures of the heating cycles were determined by analyses of second derivative curves (Tauxe, 1998). To resolve the component of the natural remanent magnetization (NRM) stepwise thermal demagnetization up to 400 °C was performed on 96 oriented specimens. We adopted initial steps of 50°C reduced to 25°C from 250°C onward. These data are integrated with the results obtained by three-axes stepwise alternating field (AF) demagnetization of 73 oriented specimens up to 90 mT. In 16 specimens the complete spectrum of magnetic components could not be resolved and no stable characteristic remanent magnetization (ChRM) linearly trending to the origin could be identified. In these cases the resulting magnetization great circles where combined with stable endpoint data (McFadden & McElhinny, 1988). Analyses of the samples from the mid-Waipara River were performed at the paleomagnetic laboratory of the Ludwig-Maximilian University (Munich, Germany). Details about the analyses of the discrete samples from ODP Site 1172, conducted at the paleomagnetic laboratory of the Scripps Institution of Oceanography (La Jolla, CA, USA), are described in the supporting information attached to the online version of this paper.

2.3. Biostratigraphy

2.3.1. Foraminifera

Approximately 500 g of sediment from 102 samples from the 2003, 2007 and 2012 collections was washed over a 75 μm screen. The residues were then dried, reweighed and half was retained for quantitative census work. The remaining residue was qualitatively picked for a comprehensive faunal assemblage utilized for biostratigraphy. All material is lodged in the Paleontology Collection at GNS Science, Lower Hutt, New Zealand. The focus in this study was to confirm the position of Eocene NZS boundaries, from the upper Waipawan to lower Bortonian, which are primarily based on foraminiferal biostratigraphy (Cooper, 2004; Raine et al., 2015).

2.3.2. Calcareous nannofossils

Smear slides for calcareous nannofossils were made directly from 38 samples from the 2007 and 2012 collections using standard techniques (Bown and Young, 1998). In some cases, samples contained a large amount of coarse material and strewn slides were prepared (Bown and Young, 1998). All material is lodged in the Paleontology Collection at GNS Science. Slides were analyzed using an Olympus BX53 microscope at 1000x magnification in plane-transmitted light (PL), cross-polarized light (XPL) and phase-contrast (PC) light. Taxonomic concepts for species follow that of Perch-Nielsen (1985) and (Bown, 1998, 2005). The standard scheme of Martini (NP zones; 1971) is adopted for the nannofossil biostratigraphy. Semi-quantitative analysis was completed on 34 samples in order to determine the position of key marker species.

2.3.3. Dinoflagellate cysts

A total of 51 samples from the 2007 and 2012 sample collections were processed using standard palynological processing techniques. Between 21 and 31 g of sediment were crushed, dried and the carbonate and siliceous component removed by adding hot 10% HCl and 50% HF, respectively. Samples were then oxidized using 70% HNO_3, and washed with 5% NH_4OH to disaggregate amorphous and organic debris. Some samples were placed in an ultrasonic bath (for up to 1 minute) prior to sieving. All samples were then sieved over a 6 μm mesh, and well-mixed representative fractions of the >6 μm residue mounted on glass slides using a glycerine jelly medium. All material is lodged in the Paleontology Collection as GNS Science. Qualitative examination was completed on 30 samples, with a focus on recording the presence of taxa with biostratigraphic importance.

3. Results

3.1. Rock magnetism

Rock magnetic analyses indicate that the dominant magnetic mineral of the Ashley Mudstone is most likely greigite. The IRM backfield acquisition curves are characterized by a steep increase of magnetization up to ~150 mT, reaching the saturation magnetization (M_s) at ~300–400 mT (Figure 2a). The resulting coercivity of remanence (B_{cr}) ranges between 39 and 47 mT. These values are slightly lower than the range of 45–95 mT for sedimentary greigite reported by Roberts (1995). This can be the result of a combination of single domain (SD) and multi domain (MD) magnetic grains: Roberts et al. (2011) show that SD-dominated reference specimens possess higher B_{cr} values (75 mT) while MD-dominated are generally characterized by much lower B_{cr} values (12.6–24.5 mT). The MDF of the M_s, which varies between 20 and 30 mT (Figure 2b), is also higher than the value measured for typical MD greigite samples (i.e. < 8 mT; Roberts et al., 2011), indicating a contribution of magnetic grains with higher coercivity (i.e. SD or pseudo-SD). The thermomagnetic curves (Figure 2c) show an initial small decline of magnetization from room temperature up to ~100 °C, likely related to a minor goethite contribution that, however, is not visible in the IRM acquisition curve. A break in slope at about 200 °C is then observed, which reaches a minimum of magnetization between ~350–450 °C. This minimum is followed by an increase in magnetization that peaks at ~500 °C and decays completely at ~580°C, approximately the Curie temperature of magnetite.

The thermomagnetic curves are irreversible, and the cooling curves are characterized by a magnetization that, back at room temperature, is four to nine times higher than the initial value before heating. These curves are very similar in shape to those observed in the greigite-bearing sediments described by

Roberts (1995) and generally to the representative curves selected by Roberts et al. (2011). The minimum of magnetization between 300 °C and 400 °C is a common feature of thermomagnetic experiments of samples containing greigite, which irreversibly breaks down during heating above ~280 °C. The peak of magnetization observed at ~500 °C is due to the formation of magnetite, which is the dominant magnetic phase observed in the cooling cycle. The presence of greigite as carrier of the NRM is also supported by the strong gyro remanent magnetization (GRM) observed during AF demagnetization (see below).

3.2. Paleomagnetism

The intensity of the NRM ranges from 1.3 x 10^{-5} to 1.9 x 10^{-4} A/m, with an average value of 7.4 x 10^{-5} A/m. No particular trends are observed across the section. A highly scattered 'A' magnetic overprint, statistically oriented N-and-up in geographic coordinates (i.e. close to the expected geocentric axial dipole direction), have been observed during AF demagnetization generally up to 12 mT, as well as during thermal demagnetization up to 150–200 °C (Figure 3a-j). In 52% ($^{38}/_{73}$) of the specimens demagnetized with the AF routine, a ChRM component trending to the origin of the orthogonal projection has been isolated at alternating fields up to 25–30 mT (Figure 3a-d). Typically from 30–40 mT and up, the specimens acquire (although with different magnitude) a GRM, highlighted with gray arrows in Figure 3e-f. GRM is a characteristic of SD material, but its magnitude in greigite is larger than in other magnetic mineral that occurs in sediments (Roberts et al., 2011). Similar behavior has been observed by Rowan and Roberts (2006) in greigite-bearing Neogene marine sediments from the Mahia Peninsula, New Zealand, as well as in many other studies on magnetically similar sediments (e.g., Florindo et al., 2007; Hu et al., 1998; Roberts et al., 2011; Sagnotti and Winkler, 1999; Sagnotti et al., 2010; Snowball, 1997a, 1997b; Stephenson and Snowball, 2001).

In 15% ($^{11}/_{73}$) of the AF-demagnetized specimens the occurrence of the GRM did not allow a successful isolation of a ChRM component directly trending to the origin of the orthogonal projection. The demagnetization pattern of these specimens is consistent with the ChRM directions pointing South-and-down and plots along a great circle (Figure 3e, f). In 52% ($^{50}/_{96}$) of the thermally demagnetized specimens, a ChRM component directly trending to the origin of the orthogonal projection has been isolated up to a temperature of 325 °C (Figure 3g, h). In 4 of the 96 specimens the thermal demagnetization patterns track along a great circle path (Figure 3i). We combine these great circles, along with the ones obtained by the AF demagnetization, with the SW-and-downward pointing stable endpoint directions applying the McFadden and McElhinny (1988) algorithm (Figure 3k).

After AF and thermal demagnetization analyses, ChRM directions were isolated by linear interpolation or estimated by great circles analyses on 61% ($^{103}/_{169}$) of all the specimens. These directions are organized in two modes statistically oriented NE-and-Up and SW-and-Down in geographic coordinates (Figure 3l). The average directions of the two modes, calculated using the spherical statistic of Fisher (1953; Table 2) depart from antipodality by 16.4° and fail the reversal test of Watson (1983) at a 95% level of confidence (V_w=13.4; $V_{critical}$=6.2; see also Tauxe et al., 2010 for details on the method). This may be due to the presence of an unresolved magnetic bias. We minimized this effect on the average directions by inverting all directions to a common NE-and-up pointing polarity. After correction for a 22° dip directed 122°N, we obtain a mean direction of Dec.=16.2°, Inc.=-47.0° (Figure 3m, Table 2).

We calculated the position of the virtual geomagnetic pole (VGP) for each ChRM direction, and we used the latitude of each VGP relative to the mean paleomagnetic north pole for interpreting the magnetic polarity stratigraphy (Kent et al., 1995; Lowrie and Alvarez, 1977). A total of 35 sedimentary layers have 2 to 3 ChRM directions that have been used to calculate site mean directions. The VGP relative latitudes approaching +90° or -90° are interpreted as recording normal or reverse polarity, respectively (Figure 4). These data show a ~7 m-thick stratigraphic interval of normal magnetic polarity including a brief reverse polarity interval of about 1.3 m at about 7 m. This is followed by ~12 m of mainly reversed polarity, interrupted by a one sample-based normal polarity event at 13.6 m. From 20.8 m to 31.4 m the sediments were deposited during a normal polarity time interval. Reverse polarity characterizes then the section up to 41.5 m, where the last layer show again normal polarity field (Figure 4).

3.3. Biostratigraphy

In the section examined, three early–middle Eocene NZS boundaries are recognized based on planktic and benthic foraminiferal biostratigraphy (Figure 5). The Waipawan/Mangaorapan boundary, defined by the lowest occurrence (LO) of *Morozovella crater*, lies between -3.99 m (M34/f892) and -2.87 m (M34/f891). The Mangaorapan/Heretaungan boundary, defined by the LO of *Elphidium hampdenense*, is recorded between 26.75 m (M34/f993) and 27.51 m (M34/f994). The base of the Bortonian, defined by the LO of *Globigerinatheka index*, is between 58.55 m (M34/f1039) and 59.71 m (M34/f1040). The key biostratigraphic datum for the Porangan Stage, which lies between the Heretaungan and Bortonian NZS, is the benthic species *Elphidium saginatum*. This species was not recorded and suggests the Porangan Stage is missing and that an unconformity lies between the uppermost Heretaungan and lowermost Bortonian samples (Figure 5). A marked lithological change is also seen between 58.55 m and 59.71 m; from fine sand with a low component of glauconite, to sediment dominated by medium to coarse glauconite.

Calcareous nannofossil assemblages are well preserved in most of the section, although a notable decline in nannofossil preservation is seen in the upper part, from ~49.52 m (M34/f1031). In the lower part of the section, the LOs of *Tribrachiatus orthostylus* and *Sphenolithus radians* between -13.2 m (M34/895) and -6.61 m (M34/f894) mark the base of calcareous nannofossil zone NP11 (Figure 5). The LO of *Discoaster lodoensis* between -3.99 m (M34/f892) and -2.87 m (M34/f891) marks the base of zone NP12. The highest occurrence (HO) of *T. orthostylus* between 11.13 m (M34/f959) and 12.55 m (M34/f963) marks the base of NP13. It is difficult to position the NP13/NP14 boundary due to the absence of *Discoaster sublodoensis,* which marks the base of zone NP14. Samples from 12.55 m (M34/f0963) to 58.55 m (M34/f1039) are therefore assigned to a combined NP13/14 zone. Nannofossil biostratigraphy supports foraminiferal evidence that time is missing between 58.55 m (M34/f1039) and 62.26 m (M34/f1043). The FO of *Nannotetrina fulgens* marks the base of NP15, but the absence of this taxon, combined with the absence of *Chiamolithus gigas*, which LO and HO mark respectively base and top of Subzone NP15b, indicates that NP15 is not present at mid-Waipara. The LOs of

Reticulofenestra umbilicus and *R. reticulata,* both key markers for zone NP16, are recorded at 62.26 m (M34/f1043).

Several dinocyst biostratigraphic events were recorded through the section (Figure 5). In the lower part of the section, the HO of *Samlandia delicata* is recorded between -16.15 m (M34/f899) and -15.25 m (M34/f898), the LO of *Dracodinium waipawaense* between -13.2 m (M34/895) and -6.61 m (M34/f894), the LO of the genus *Homotryblium* between -6.61 m (M34/f894) and -5.11 m (M34/f893), and the LO of *Wilsonidium ornatum* between -5.11 m (M34/f893) and -3.99 m (M34/892). From the 2012 collection, important dinocyst bioevents recorded are the HO of *Wilsodinium ornatum* between 14.01 m (M34/f967) and 16.43 m (M34/f971), the HO of the genus *Apectodinium* and the LO of *Charlesdowniea coleothrypta* between 17.83 m (M34/f975) and 19.98 m (M34/f979), the LO of *Charlesdowniea edwardsii* between 19.98 m (M34/f979) and 22.14 m (M34/f985), and the HO of *C. edwardsii* between 32.4 m (M34/f1005) and 35.08 m (M34/f1010).

4. Discussion

4.1. Mid-Waipara age model and magneto-biochronology

Biostratigraphic data from the mid-Waipara River section provides a first indirect correlation with the international GTS12 timescale (Figure 6). In particular for the lower part of the section, where no magnetic polarity data is available, we correlated the section with the GTS12 timescale using the LO of *Samlandia delicata, Tribrachiatus orthostylus*, and *Morozovella crater*. The LO of *S. delicata*, between -16.15 m and -15.25 m, provides the best calibration point for the base of the section. At mid-Waipara, and also the Tawanui section in the East Coast Basin, New Zealand, *S. delicata* is first recorded within nannofossil Zone NP10. For the LO of *T. orthostylus*, a recent age calibration in a Southwest Pacific setting has been obtained from the Mead Stream section in the Marlborough region, New Zealand (Dallanave et al., 2015). Here the LO of *T. orthostylus* occurred within the upper part of Chron C24r, with an age assignment of 54.72 Ma. The position with respect to the GPTS observed at Mead Stream is in agreement with data from the Belluno Basin, and from ODP Site 1262, Leg 208, southeast Atlantic Ocean (Agnini et al., 2007); the latter was used by Gradstein et al. (2012) to calibrate the age of the B (base) of *T. orthostylus*. The LO of *M. crater* is recorded at Mead Stream close to the C23r/C23n Chron boundary (51.91 Ma; Dallanave et al., 2015). Using this data from Mead Stream, along with the position at mid-Waipara and linear extrapolation with the magnetostratigraphically well-constrained interval overlying this part of the section, suggests the LO of *M. crater* corresponds to ~52.0 Ma (Raine et al., 2015). As previously mentioned, the LO of *M. crater* defines the base of the Mangaorapan NZS (Cooper, 2004; Raine et al., 2015).

Applying a correlation line that incorporates the three bioevents (LO of *M. crater*, *T. orthostylus* and *S. delicata*) in the lower part of the section (Figure 6), an estimated age of ~55.5 Ma for the LO of *S. delicata* is predicted.

In the upper part of the mid-Waipara River section (2012 collection) two biostratigraphic events have been used for a first correlation with the GTS12 time scale. The first is the HO of *Tribrachiatus orthostylus*, which defines the base of nannofossil Zone NP13. At Mead Stream it has been found to occur within Chron C22r (Dallanave et al., 2015), as well as in the Belluno Basin, where the same event has been found in the lower part of Chron C22r (Agnini et al., 2006, 2014). Up-section, the LO of *Elphidium hampdenense*, which defines the base of the Heretaungan NZS, has been indirectly placed within Chron 22n (Hollis et al., 2010). Following these biostratigraphic constraints we can correlate the series of six magnetic polarity reversals retrieved in the mid-Waipara sediments (Figures 2 and 4) with Chrons C23n.2n–C21n (~51.5–47 Ma).

In the uppermost part of the section, there appears to be an unconformity between 58.55 m (M34/f1039) and 59.71 m (M34/f1040). Sediment at 58.55 m is dated as Heretaungan by foraminifera and calcareous nannofossils (Figure 6). However, samples immediately overlying record the LO of the Bortonian NZS marker *Globigerinatheka index* (59.71 m), the LOs of zone NP16 species *Reticulofenestra umbilicus* and *R. reticulata* (62.26 m), and a marked coarsening of sediment with abundant medium to coarse glauconite (59.71 m). The LO of *G. index* is placed at 42.6 Ma (Raine et al., 2015), while the LO of *R. umbilicus* and *R. reticulata* is dated at 42.9 Ma (Gradstein et al., 2012), indicating that at least 3 Myr of sedimentary record, including the Porangan NZS and Zone NP15, are missing.

We have used all the discussed tie points to construct an age-depth plot and derive a sediment accumulation rate (SAR) of the sediment, and have also assumed a constant sedimentation rate between each pair of chronologic control points (Figure 6). The SAR ranges from 3.5to 13.6 m/Myr, with an average of 7.4 m/Myr. The age-depth plot is used to derive the ages for the selected biostratigraphic datums that occur within the section (Figure 6, Table 2). It is worth noting that the lowest SAR of 3.5 m/Myr is not entirely reliable, given that magnetic polarity data has not been completed in the lower part of the section.

For the first time, the base of the Heretaungan NZS, defined by the LO of *E. hampdenense*, is magnetostratigraphically-calibrated, and placed at C22n(0.6), i.e., 48.88 Ma (GTS12). This age is ~230 kyr younger than the 49.11 Ma age inferred by Hollis et al. (2010; recalibrated with respect to the GTS12 timescale) from indirect calibration of the LO of *E. hampdenense* to the LO of nannofossil *D. sublodoensis* (Berggren et al., 1995).

4.2. Correlation with Southern Ocean records

The robust magnetostratigraphic framework we have established for the mid-Waipara section provides a means to improve correlation with ODP Site 1172 and IODP Site U1356. Of the three groups of microfossil studied at mid-Waipara, only the dinocysts occur throughout the sedimentary successions at all three sites. Therefore, we have utilized the newly calibrated dinocyst datums at mid-Waipara to reassess the age determination for Sites 1172 and U1356.

At Site 1172, our discrete samples-based paleomagnetic analysis (see supporting material) shows that, at least for the early and middle Eocene part of the core, it is not possible to construct any reliable magnetic polarity-based chronology. To correlate the record from Site 1172 with mid-Waipara, we use several tie points. The first is the Paleocene–Eocene boundary, defined by the onset of a global negative carbon isotope excursion (CIE), which is well recorded in the sediments of Site 1172 (611.89 mbsf; Sluijs et al., 2011). In addition, we use the LO of *Samlandia delicata,* the HO of *Wilsonidium ornatum*, the LO of *Charlesdowniea edwardsii*, and the HO of *C. edwardsii*, which are all calibrated at mid-Waipara and well constrained at Site 1172 (Bijl et al., 2013b)(Figure 5).

At Site U1356 paleomagnetic results between ~958 mbsf to 1000 mbsf and the correlation with Chrons C24n proposed by Tauxe et al. (2012) are considered reliable (Figure 5). Between ~940 and 949 mbsf dinocyst biostratigraphy indicate the presence of a major unconformity (Bijl et al., 2013b). Upcore, the recovery is very limited and paleomagnetic interpretation is complicated by discrepancies between archive halves and discrete samples results, clearly visible (e.g.) at ~940 mbsf. In the recovered sediment between ~929 and 933 mbsf a reliable reverse polarity interval, defined by several archive half directions and a discrete sample, is comprises between two short normal polarity levels based respectively on one discrete sample and three archive half directions. This interval can possibly represents Chron C22r. This would be in agreement with the magneto-biostratigraphic data from mid Waipara, where the HO of *Wilsondinium ornatum* has been observed within this Chron. The LO of *Charlesdowniea edwardsii* is observed at Site U1356 in a reliable normal polarity interval (~924 mbsf) interpreted by Tauxe et al. (2012) as Chron C22n, in agreement with data from mid-Waipara. Accordingly to the dinocyst zonation compiled by Bijl et al. (2013b) for Sites 1172 and U1356, the HO of *Wilsondinium ornatum* and The LO of *Charlesdowniea edwardsii* appear to be diachronous, occurring within dinocyst Zone SPDZ8 at Site U1356 and within Zone SPDZ7 at Site 1172, being thus ~1 Myr younger at Site U1356. Nonetheless, basing the correlation between the two sites on the generic SPDZ8 Zone rather than the these two specific events, the magnetostratigraphic data of Site U1356 would be even more difficult to reconcile with the GPTS, since SPDZ8 Zone at Site 1172 is almost entirely included in a reverse polarity zone (i.e. Chron C21r, determined by correlation with mid-Waipara; Figure 7). TEX_{86} data from this part of Site U1356 are however very few and spares (Figure 7), and both these age assignation for the ~920–940 mbsf part of Site U1356 would not affect the overall paleoclimate trend discussed below.

4.3. Paleotemperature proxy records

In order to put the paleotemperature proxy record of Site U1356 and Site 1172 on a time frame together with the record from mid-Waipara, we used the correlation points listed above to construct an age-model of sedimentation for both the Sites (Figure 7).

At Site 1172, a hiatus removing dinocyst zones SPDZ4–5 has been observed at ~588 mbsf (Bijl et al., 2013b; Figure 7). Below this level we interpolated the position of the Paleocene–Eocene boundary (611.89 mbsf; Sluijs et al., 2011) and the LO of *S. delicata*, estimated at ~55.5 Ma, resulting in a SAR of ~15 m/Myr. Above the hiatus we derived an average SAR of 12.8 m/Myr by linear interpolation of the HO of *W. ornatum*, and LO and HO of *C. edwardsii*.

At Site U1356 a linear interpolation of the C24n Chron boundaries between ~1000 and 948 mbsf results in an average SAR of 25.8 m/Myr. Between ~948 and 940 mbsf, a hiatus completely removes dinocyst zone SPDZ6–7 (Bijl et al., 2013b). Above, sediment recovery is very low. Assuming the same SAR is recorded across C24n through the HO of *W. ornatum* and LO of *C. edwardsii*, found within Chron C22 at mid-Waipara, the estimated duration of the hiatus results in ~1.6 Myr, similar to that estimated by Tauxe et al. (2012; see also Bijl et al., 2013b). Correlating this part of the sections with the age model of Site 1172 using Zone SPDZ8 rather than HO of *W. ornatum* and LO of *C. edwardsii* as described above, would result in an estimated hiatus of ~3.5 Myr. It would make anyway difficult to correlate the available magnetic polarity data from Site U1356 with the GPTS, as shown in Figure 7.

We used the age model for the mid-Waipara River section, Site U1356, and Site 1172 to compare the TEX_{86} proxy records from the three localities. The TEX_{86} record from these three sites have previously been used to reconstruct the temperature history of the southwest Pacific and Southern Ocean during the early and middle Eocene (Bijl et al., 2009, 2010, 2013a; Hollis et al., 2009, 2012). Hollis et al. (2012) demonstrated that TEX_{86} values are a robust guide to relative temperature variation in the mid-Waipara and ODP Site 1172 records. They also showed that of the two calibrations introduced by Kim et al. (2010), the TEX^{L}_{86} provides the best fit in terms of absolute temperature values with other temperature proxies in middle to high latitude localities. However, the glycerol dibiphytanyl glycerol tetraethers (GDGTs) distribution that underlies this calibration suffers from poorly understood variations in some settings that can cause anomalous temperature values (Taylor et al., 2013). For this reason, we use the less ambiguous relative SST proxy, TEX_{86}, to investigate how well our age models perform in capturing the sea temperature history of the Southwest Pacific and Southern Ocean.

The combined TEX_{86} dataset reveal a sharp increase of paleotemperature that peaking between ~54–53 Ma with the data from Site U1356. This maximum seems to anticipate the commonly accepted age of ~52–50 Ma for the EECO based on the global benthic $\delta^{18}O$ record (Zachos et al., 2008; Figure 8). Relying on the robustness of the age model for this part of Site U1356 (i.e., ~968–1000 mbsf, Figure 7), this could be firstly due to a mixing of terrestrial and marine lipid influencing the TEX_{86} data. A Branched and Isoprenoid Tetraether (BIT) cutoff of 0.4, as used by Bijl et al. (2013a) for this record, cannot exclude contamination from terrestrial material (Hopmans et al., 2004), which can also explain the high dispersion of the data. Secondly, the paucity of TEX_{86} data in the compiled record between 52.2 and 50.5 Ma does not allow to define clearly the trend during this interval. However, data from mid-Waipara suggests that the warm condition persisted to 50 Ma, in agreement with the global benthic $\delta^{18}O$ record. The TEX_{86} values then indicate the inset of a general cooling. The similarity of the mid-Waipara and the Site 1172 record give us confidence about the reliability of our age model. This trend is punctuated by short-lived warming events, which may prove to be post-EECO equivalents to the post-PETM hyperthermals.

5. Conclusions

We present a new integrated magneto-biostratigraphic chronology for the Southwest Pacific Ocean spanning the early-middle Eocene (~56–45 Ma). This has been constructed using a robust magnetostratigraphy from the Mid-Waipara River section integrated with foraminifera, calcareous nannofossil, and dinocyst biostratigraphy. In this framework we provide the first magnetostratigraphically-calibrated age of 48.88 Ma for the Mangaorapan/Heretaungan New Zealand Stage boundary, which is defined by the LO of the benthic foraminifera *Elphidium hampdenense.* This result improves the calibration of the early to middle Eocene New Zealand time scale and associated bioevents with the current international time scale (GTS12).

Paleomagnetic analyses conducted on discrete samples from ODP Site 1172 underscore the poor reliability of most of the previously published early–middle Eocene magnetic polarity record and age models for this site. We reinforced the age calibration of ODP Site 1172 and IODP Site U1356 by means of dinocyst biostratigraphy correlation with the mid-Waipara record. This allows a review of the timing of climate events and trends in the Southwest Pacific and Southern Ocean by comparing the TEX_{86} SST proxy record from these three different localities. The re-calibrated climate history exhibits a general close agreement between regions, but underlies the possible contamination from terrestrial lipid of the TEX_{86} record of the Wilkes Land Margin. Data from mid-Waipara and Site 1172 show also a very good agreement with the global benthic $\delta^{18}O$ record of deep sea temperatures (Zachos et al., 2008), constraining the time of the post-EECO global cooling also in the Southwest Pacific.

References

Agnini, C., Fornaciari, E., Raffi, I., Catanzariti, R., Pälike, H., Backman, J., Rio, D., 2014. Biozonation and biochronology of Paleogene calcareous nannofossils from low and middle latitudes. Newsletters Stratigr. 47, 131–181.

Agnini, C., Fornaciari, E., Raffi, I., Rio, D., Röhl, U., Westerhold, T., 2007. High-resolution nannofossil biochronology of middle Paleocene to early Eocene at ODP Site 1262: Implications for calcareous nannoplankton evolution. Mar. Micropaleontol. 64, 215–248.

Agnini, C., Muttoni, G., Kent, D. V., Rio, D., 2006. Eocene biostratigraphy and magnetic stratigraphy from Possagno, Italy: The calcareous nannofossil response to climate variability. Earth Planet. Sci. Lett. 241, 815–830.

Berggren, W.A., Kent, D. V., Swisher, C.C.I., Aubry, M.-P., 1995. A revised Cenozoic geochronology and chronostratigraphy, in: Berggren, W.A., Kent, D. V., Aubry, M.-P., Hardenbol, J. (Eds.), Geochronology, Time Scales and Global Stratigraphy Correlation: A Unified Temporal Framework for a Historical Geology. Society of Economic Paleontologist and Mineralogist Special Pubblication No. 54, Tulsa, pp. 129–213.

Bijl, P.K., Bendle, J.A.P., Bohaty, S.M., Pross, J., Schouten, S., Tauxe, L., Stickley, C.E., McKay, R.M., Röhl, U., Olney, M., Sluijs, A., Escutia, C., Brinkhuis, H., 2013a. Eocene cooling linked to early flow across the Tasmanian Gateway. Proc. Natl. Acad. Sci. U. S. A. 110, 9645–50.

Bijl, P.K., Houben, A.J.P., Schouten, S., Bohaty, S.M., Sluijs, A., Reichart, G.-J., Sinninghe Damsté, J.S., Brinkhuis, H., 2010. Transient Middle Eocene atmospheric CO_2 and temperature variations. Science 330, 819–21.

Bijl, P.K., Schouten, S., Sluijs, A., Reichart, G.-J., Zachos, J.C., Brinkhuis, H., 2009. Early Palaeogene temperature evolution of the southwest Pacific Ocean. Nature 461, 776–779.

Bijl, P.K., Sluijs, A., Brinkhuis, H., 2013b. A magneto- and chemostratigraphically calibrated dinoflagellate cyst zonation of the early Palaeogene South Pacific Ocean. Earth-Science Rev. 124, 1–31.

Bown, P.R., 1998. Calcareous Nannofossil Biostratigraphy. Cambridge University Press, Cambridge, UK.

Bown, P.R., 2005. Palaeogene calcareous nannofossils from the Kilwa and Lindi areas of coastal Tanzania (Tanzania Drilling Project Sites 1 to 10, 2003-4). J. Nannoplankt. Res. 27, 21–95.

Bown, P.R., Young, J.R., 1998. Techniques, in: Bown, P.R. (Ed.), Calcareous Nannofossil Biostratigraphy. British Micropaleontological Society Publications Series. Springer Sciences+Business Media, LLC, New York, USA, pp. 16–21.

Burgess, C.E., Pearson, P.N., Lear, C.H., Morgans, H.E.G., Handley, L., Pancost, R.D., Schouten, S., 2008. Middle Eocene climate cyclicity in the southern Pacific: Implications for global ice volume. Geology 36, 651–654.

Creech, J.B., Baker, J.A., Hollis, C.J., Morgans, H.E.G., Smith, E.G.C., 2010. Eocene sea temperatures for the mid-latitude southwest Pacific from Mg/Ca ratios in planktonic and benthic foraminifera. Earth Planet. Sci. Lett. 299, 483–495.

Crouch, E.M., Brinkhuis, H., 2005. Environmental change across the Paleocene-Eocene transition from eastern New Zealand: A marine palynological approach. Mar. Micropaleontol. 56, 138–160.

Dallanave, E., Agnini, C., Bachtadse, V., Muttoni, G., Crampton, J.S., Strong, C.P., Hines, B.R., Hollis, C.J., Slotnick, B.S., 2014. Early to middle Eocene magneto-biochronology of the southwest Pacific Ocean and climate influence on sedimentation: Insights from the Mead Stream section, New Zealand. Geol. Soc. Am. Bull. 1–18.

Dallanave, E., Agnini, C., Bachtadse, V., Muttoni, G., Crampton, J.S., Strong, C.P., Hines, B.R., Hollis, C.J., Slotnick, B.S., 2015. Early to middle Eocene magneto-biochronology of the southwest Pacific Ocean and climate influence on sedimentation: Insights from the Mead Stream section, New Zealand. Geol. Soc. Am. Bull. 127, 643–660.

Fisher, R., 1953. Dispersion on a sphere. Proc. R. Soc. London A217, 295–305.

Florindo, F., Karner, D., Marra, F., Renne, P., Roberts, A.P., Weaver, R., 2007. Radioisotopic age constraints for Glacial Terminations IX and VII from aggradational sections of the Tiber River delta in Rome, Italy. Earth Planet. Sci. Lett. 256, 61–80.

Fuller, M., Touchard, Y., 2004. On the magnetostratigraphy of the East Tasman Plateau Timing of the opening of the Tasmanian Gateway and paleoenvironmental changes, in: Exon, N.F., Kennet, J.P., Malone, M.J. (Eds.), The Cenozoic Southern Ocean: Tectonics, Sedimentation, and Climate Change Between Australia and Antarctica, Geophys. Monogr. Ser., Vol. 151. Washington DC, USA, pp. 63–78.

Gradstein, F.M., Ogg, J.G., Schmitz, M.D., Ogg, G.M., 2012. The Geologic Time Scale 2012. Elsevier.

Hollis, C.J., Beu, A.G., Crampton, J.S., Crundwell, M.P., Morgans, H.E.G., Raine, J.I., Jones, C.M., Boyes, A.F., 2010. Calibration of the New Zealand Cretaceous-Cenozoic Timescale to GTS2004. GNS Sciences Report, 2010/43.

Hollis, C.J., Dickens, G.R., Field, B.D., Jones, C.M., Strong, C.P., 2005. The Paleocene–Eocene transition at Mead Stream, New Zealand: A southern Pacific record of early Cenozoic global change. Palaeogeogr. Palaeoclimatol. Palaeoecol. 215, 313–343.

Hollis, C.J., Handley, L., Crouch, E.M., Morgans, H.E.G., Baker, J.A., Creech, J.B., Collins, K.S., Gibbs, S.J., Huber, M., Schouten, S., Zachos, J.C., Pancost, R.D., 2009. Tropical sea temperatures in the high-latitude South Pacific during the Eocene. Geology 37, 99–102.

Hollis, C.J., Taylor, K.W.R., Handley, L., Pancost, R.D., Huber, M., Creech, J.B., Hines, B.R., Crouch, E.M., Morgans, H.E.G., Crampton, J.S., Gibbs, S., Pearson, P.N., Zachos, J.C., 2012. Early Paleogene temperature history of the Southwest Pacific Ocean: Reconciling proxies and models. Earth Planet. Sci. Lett. 349-350, 53–66.

Hopmans, E.C., Weijers, J.W.H., Schefuß, E., Herfort, L., Sinninghe Damsté, J.S., Schouten, S., 2004. A novel proxy for terrestrial organic matter in sediments based on branched and isoprenoid tetraether lipids. Earth Planet. Sci. Lett. 224, 107–116.

Hu, S., Appel, E., Hoffmann, V., Schmahl, W.W., Wang, S., 1998. Gyromagnetic remanence acquired by greigite (Fe3S4) during static three-axis alternating field demagnetization. Geophys. J. Int. 134, 831–842.

Huber, M., Nof, D., 2006. The ocean circulation in the southern hemisphere and its climatic impacts in the Eocene. Palaeogeogr. Palaeoclimatol. Palaeoecol. 231, 9–28.

Huber, M., Sloan, L.C., 2001. Heat transport, deep waters, and thermal gradients: Coupled simulation of an Eocene greenhouse climate. Geophys. Res. Lett. 28, 3481–3484.

Kent, D. V., Olsen, P.E., Witte, W.K., 1995. Late Triassic-erliest Jurassic geomagnetic polarity sequence and paleolatitudes from drill cores in the Newark rift basin, eastern North America. J. Geophys. Res. 100, 14965–14998.

Krása, D., Petersen, K., Petersen, N., 2007. Variable field translation balance, in: Gubbins, D., Herrero-Bervera, E. (Eds.), Encyclopedia of Geomagnetism and Paleomagnetism. Springer, pp. 977–979.

Lowrie, W., Alvarez, W., 1977. Upper Cretaceous–Paleocene magnetic stratigraphy at Gubbio, Italy: III. Magnetic stratigraphy. Geol. Soc. Am. 88, 374–377.

Martini, E., 1971. Standard Tertiary and Quaternary calcareous nannoplankton zonation., in: Farinacci, A. (Ed.), Proceedings of the 2nd International Conference Planktonic Microfossils. Edizioni Tecnoscienza, Rome, pp. 739–785.

McFadden, P.L., McElhinny, M.W., 1988. The combined analysis of remagnetization circles and direct observations in palaeomagnetism. Earth Planet. Sci. Lett. 87, 161–172.

Miller, K.G., Wright, J.D., Fairbanks, R.G., 1991. Unlocking the Ice House: Oligocene-Miocene oxygen isotopes, eustasy, and margin erosion. J. Geophys. Res. 96, 6829.

Morgans, H.E.G., Jones, C.M., Crouch, E.M., Field, B.D., Raine, J.I., Strong, C.P., Wilson, G.J., 2005. Upper Cretaceous to Eocene stratigraphy and sample collections , mid-Waipara River section , North Canterbury. Institute of Geological & Nuclear Sciences report 2003/08.

Pancost, R.D., Taylor, K.W.R., Inglis, G.N., Kennedy, E.M., Handley, L., Hollis, C.J., Crouch, E.M., Pross, J., Huber, M., Schouten, S., Pearson, P.N., Morgans, H.E.G., Raine, J.I., 2013. Early Paleogene evolution of terrestrial climate in the SW Pacific, Southern New Zealand. Geochemistry, Geophys. Geosystems 14, 1–17.

Perch-Nielsen, K., 1985. Cenozoic calcareous nannofossils, in: Bolli, H.M., Saunders, J.B., Perch-Nielsen, K. (Eds.), Plankton Stratigraphy. Cambridge University Press, Cambridge, UK, pp. 427–554.

Pross, J., Contreras, L., Bijl, P.K., Greenwood, D.R., Bohaty, S.M., Schouten, S., Bendle, J.A.P., Röhl, U., Tauxe, L., Raine, J.I., Huck, C.E., van de Flierdt, T., Jamieson, S.S.R., Stickley, C.E., van de Schootbrugge, B., Escutia, C., Brinkhuis, H., 2012. Persistent near-tropical warmth on the Antarctic continent during the early Eocene epoch. Nature 488, 73–7.

Raine, J.I., Campbell, H.J., Crundwell, M.P., Beu, A.G., Cooper, R.A., Hollis, C.J., Boyes, A.F., Crampton, J.S., 2015. Revised calibration of the New Zealand Geological Timescale: NZGT2015/1. GNS Sciences Report, 2012/39., Lower Hutt, New Zealand.

Roberts, A.P., 1995. Magnetic properties of sedimentary greigite (Fe3S4). Earth Planet. Sci. Lett. 134, 227–236.

Roberts, A.P., Chang, L., Rowan, C.J., Horng, C.S., Florindo, F., 2011. Magnetic properties of sedimentary greigite (Fe3S4): An update. Rev. Geophys. 49, RG1002.

Rowan, C.J., Roberts, A.P., 2006. Magnetite dissolution, diachronous greigite formation, and secondary magnetizations from pyrite oxidation: Unravelling complex magnetizations in Neogene marine sediments from New Zealand. Earth Planet. Sci. Lett. 241, 119–137.

Sagnotti, L., Cascella, A., Ciaranfi, N., Macrì, P., Maiorano, P., Marino, M., Taddeucci, J., 2010. Rock magnetism and palaeomagnetism of the Montalbano Jonico section (Italy): evidence for late diagenetic growth of greigite and implications for magnetostratigraphy. Geophys. J. Int. 180, 1049–1066.

Sagnotti, L., Winkler, A., 1999. Rock magnetism and palaeomagnetism of greigite-bearing mudstones in the Italian peninsula. Earth Planet. Sci. Lett. 165, 67–80.

Sluijs, A., Bijl, P.K., Schouten, S., Röhl, U., Reichart, G.-J., Brinkhuis, H., 2011. Southern ocean warming, sea level and hydrological change during the Paleocene-Eocene thermal maximum. Clim. Past 7, 47–61.

Snowball, I.F., 1997a. The detection of single-domain greigite (Fe3S4) using rotational remanent magnetization (RRM) and the effective gyro field (Bg): mineral magnetic and palaeomagnetic applications. Geophys. J. Int. 130, 704–716.

Snowball, I.F., 1997b. Gyroremanent magnetization and the magnetic properties of greigite-bearing clays in southern Sweden. Geophys. J. Int. 129, 624–636.

Stephenson, A., Snowball, I.F., 2001. A large gyromagnetic effect in greigite. Geophys. J. Int. 145, 570–575.

Tauxe, L., 1998. Paleomagnetic principles and practice. Dordrecht, The Netherland.

Tauxe, L., 2010. Essentials of Paleomagnetism. University of California Press, Berkeley.

Tauxe, L., Stickley, C.E., Sugisaki, S., Bijl, P.K., Bohaty, S.M., Brinkhuis, H., Escutia, C., Flores, J.A., Houben, A.J.P., Iwai, M., Jiménez-Espejo, F., McKay, R., Passchier, S., Pross, J., Riesselman, C.R., Röhl, U., Sangiorgi, F., Welsh, K., Klaus, A., Fehr, A., Bendle, J.A.P., Dunbar, R., Gonzàlez, J., Hayden, T., Katsuki, K., Olney, M.P., Pekar, S.F., Shrivastava, P.K., van de Flierdt, T., Williams, T., Yamane, M., 2012. Chronostratigraphic framework for the IODP Expedition 318 cores from the Wilkes Land Margin: Constraints for paleoceanographic reconstruction. Paleoceanography 27, PA2214.

Taylor, K.W.R., Huber, M., Hollis, C.J., Hernandez-Sanchez, M.T., Pancost, R.D., 2013. Re-evaluating modern and Palaeogene GDGT distributions: Implications for SST reconstructions. Glob. Planet. Change 108, 158–174.

Watson, G., 1983. Large sample theory of the Langevin distribution. J. Stat. Plan. Inference 8, 245–256.

Wilson, G.J., 1988. Paleocene and Eocene dinoflagellate cysts from Waipawa, Hawkes Bay, New Zealand. New Zealand Geological Survey paleontological bulletin,0078- 8589 ;57.

Zachos, J.C., Dickens, G.R., Zeebe, R.E., 2008. An early Cenozoic perspective on greenhouse warming and carbon-cycle dynamics. Nature 451, 279–83.

Figure captions

Figure 1. A) Location of the mid-Waipara River section (South Island, New Zealand, 43.0537°S, 172.6110°E), ODP Site 1172 (Leg 189, East Tasman Plateau, 43.9598°S, 149.9283°E), and IODP Site U1356 (Exp. 318, Wilkes Land Margin, 63.3102°S, 135.9989°E). B) Paleogeographic reconstruction for the New Zealand region for the early Eocene (~56 Ma) showing the position of the mid-Waipara River, Mead Stream, and Tawanui sections; modified from Hollis et al. (2005). C) Position of the samples collected in the 2003, 2007 and the 2012 expedition, with the biostratigraphic events used to correlate the 2003 and 2012 suites; the key correlation event is the lowest occurrence (LO) of the foraminifera *Elphidium hampdenense*.

Figure 2. A) Isothermal remanent magnetization (IRM) backfield acquisition curves of representative specimens from Mid-Waipara; M/M_S= magnetization/saturation magnetization. The horizontal scale (inducing field) is

magnified from 0 to 0.5 T. B) AF demagnetization spectra of M_s of the same specimens showed in panel A; the gray band highlights the range of the M_s median destructive field. C) Representative thermomagnetic curves from Mid-Waipara sediments; M= magnetization. Dashed lines indicate the Curie temperature of the magnetic phase derived by analyses of second derivative curves (Tauxe, 1998).

Figure 3. Representative vector end point demagnetization diagrams of AF and thermal demagnetized core specimens from mid-Waipara and equal-area projections of the component directions. Filled (open) symbols on the vector end point diagrams represent projections onto the horizontal (vertical) plane, while filled (open) symbols of the equal area projections represent down (up) pointing vectors. A-d) AF demagnetized score specimens; dashed lines highlight the ChRM directions trending to the origin of the demagnetization axes; the gray thick arrow indicates the effect of the gyro remanent magnetization (GRM). E-f) AF-demagnetized specimens strongly affected by GRM (highlighted by the gray arrows); in these cases the ChRM directions were estimated by great circles analyses. G-h) Examples of thermally demagnetized specimens; in the example i) the ChRM direction lies on a great circle (shown in the equal area projection). J) Equal area projection of the ‘A’ component (overprint) directions of the NRM in geographic coordinates. The open star is the expected directions of the present-day geomagnetic field calculated the geocentric axial dipole (GAD) model (e.g. Tauxe et al., 2010). K) Down-pointing ChRM best-fit directions (black dots) combined with great circles demagnetization path (gray circles) in geographic coordinates. These data were combined following McFadden and McElhinny (1988) to estimate the ChRM directions (gray squares) from the great circles. In panel l) and m) are represented the equal area projections of all the ChRM directions before and after bedding tilt correction, respectively. The black (open) square represents the mean direction of the SW-and-down (NE-and-up) pointing directions, with the associated α_{95} confidence cone. The open diamond is the mean direction, with the associated α_{95} confidence cone, of all the directions plotted to a common up-pointing polarity.

Figure 4. Magnetic polarity stratigraphy of the mid-Waipara River section. From left to right: Lithology and thickness; natural remanent magnetization (NRM) of the core specimens; declination and inclination of the ChRM directions (or layer mean directions) and the associated virtual geomagnetic poles (VGP) latitude. The magnetic-polarity stratigraphy has been determined by means of the VGP latitudes: black (white) bars of the right column indicate normal (reverse) polarity intervals.

Figure 5. From left to right: foraminifera, calcareous nannofossil, and dinoflagellate cyst (dinocyst) biostratigraphy of the mid-Waipara River section; biostratigraphic events are indicated as lowest occurrence (LO) and highest occurrence (HO); calcareous nannofossil zonation of Martini (1971); New Zealand (NZ) and international stage boundaries, associated with the magnetic polarity stratigraphy constructed as shown in Figure 4. Biostratigraphic correlation based on dinocyst events between mid-Waipara, IODP Site U1356 and ODP Site 1172; IODP Site U1356 is represented together with the paleomagnetic data from Tauxe et al. (2012): gray diamonds in the inclinations column indicate acceptable Fisher means, while gray triangles indicate acceptable best-fit lines; dark gray dots are inclination data from the archive halves (see Tauxe et al., 2012 for details); shaded areas represent recovery gaps. Dinocyst zonations for Sites U1356 and 1172 are from Bijl et al. (2013b), Crouch and Brinkhuis (2005), and Wilson (1988). The Paleocene–Eocene boundary position at Site 1172 is from Sluijs et al. (2011).

Figure 6. Age model of sedimentation for the mid-Waipara River section constructed by means of magneto-biostratigraphic correlation with the geomagnetic polarity time scale (GTS12; Gradstein et al., 2012, integrated in figure with New Zelanad -NZ- stages); black dots are magnetic polarity-based tie points, while gray dots are biostratigraphic-based tie points; uncertain parts of the age model are shown with a dashed line. The age model has been used to derive sediment accumulation rates (SAR), plotted on the side of the mid-Waipara River magnetic polarity stratigraphy.

Figure 7. Age model of sedimentation of IODP Site U1356 and ODP Site 1172. Black dots are magnetic polarity-based tie points, while gray dots are biostratigraphic-based tie points. See text for details. (*) TEX_{86} data from each site are from Bijl et al. (2013a). See Figure 5 for sources of the dinoflagellate cyst (dinocyst) zonation. Dashed line represent the alternative age model for Site U1356 if correlated with Site 1172 through SPDZ8 dinocyst zone rather than directly with the mid-Waipara River record using the highest occurrence (HO) of *Wilsondinium ornatum* and lowest occurrence (LO) of *Charlesdowniea edwardsii*; see text for details.

Figure 8. TEX_{86} records from the mid-Waipara River section (Hollis et al., 2009, 2012), Ocean Drilling Program (ODP) Site 1172 and Integrated Ocean Drilling Program (IODP) Site U1356 (Bijl et al., 2009, 2013a). The record of Site 1172 and U1356 are recalibrated using the biostratigraphic correlation with the mid-Waipara River section described in the text. The composite southwest Pacific-Southern Ocean proxy record is compared with the global benthic $\delta^{18}O$ record of Zachos et al. (2008) recalibrated to the time scale of Gradstein et al. (2012; GTS12), in figure integrated with the New Zealand stage boundaries (Raine et al., 2015 and this work).

Table 1. List of magneto-biostratigraphic event and tie-points of the mid-Waipara River section.
LO= lowest occurrence; HO= highest occurrence; D= dinoflagellate cyst (dinocyst); N= calcareous nannofossil; F= foraminifera; (*) age assignment from Gradstein et al. (2012). Bold events or Chron boundaries are used as tie points for construction of the age model of sedimentation (shown in Figure 6).

Table 2. Characteristic remanent magnetization (ChRM) directions from the mid-Waipara River section.
N= number of directions; MAD= maximum angular deviation (°); k= Fisher (1953) precision parameter of the mean paleomagnetic direction; α_{95}= Fisher (1953) 95% confidence angle for the mean paleomagnetic direction; DEC and INC= declination and inclination of the mean paleomagnetic directions. Reverse

and normal polarity directions statistics are calculated after inverting all directions to a common NE-and-Up pointing mode.

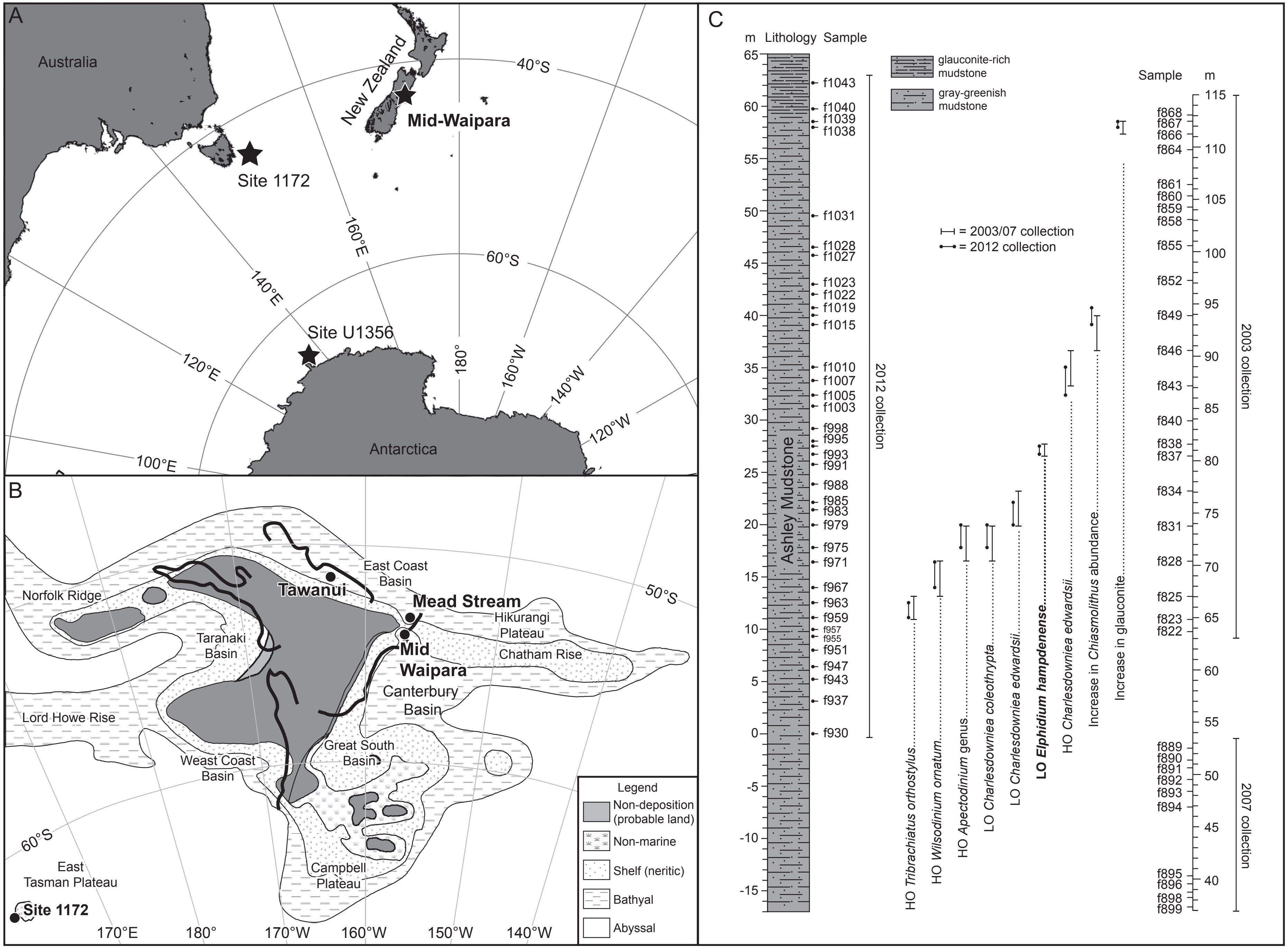

A
Australia
New Zealand
Mid-Waipara
Site 1172
Site U1356
Antarctica
40°S
60°S
160°E
140°E
120°E
100°E
180°
160°W
140°W
120°W
B
Norfolk Ridge
Taranaki Basin
Tawanui
East Coast Basin
Mead Stream
Hikurangi Plateau
Mid Waipara
Chatham Rise
Canterbury Basin
Lord Howe Rise
Weast Coast Basin
Great South Basin
Campbell Plateau
East Tasman Plateau
Site 1172
50°S
60°S
170°E
180°
170°W
160°W
150°W
140°W
Legend
Non-deposition (probable land)
Non-marine
Shelf (neritic)
Bathyal
Abyssal
C
m
Lithology
Sample
Ashley Mudstone
glauconite-rich mudstone
gray-greenish mudstone
= 2003/07 collection
= 2012 collection
2012 collection
2003 collection
2007 collection
HO Tribrachiatus orthostylus
HO Wilsodinium ornatum
HO Apectodinium genus
LO Charlesdowniea coleothrypta
LO Charlesdowniea edwardsii
LO Elphidium hampdenense
HO Charlesdowniea edwardsii
Increase in Chiasmolithus abundance
Increase in glauconite

Figure 1

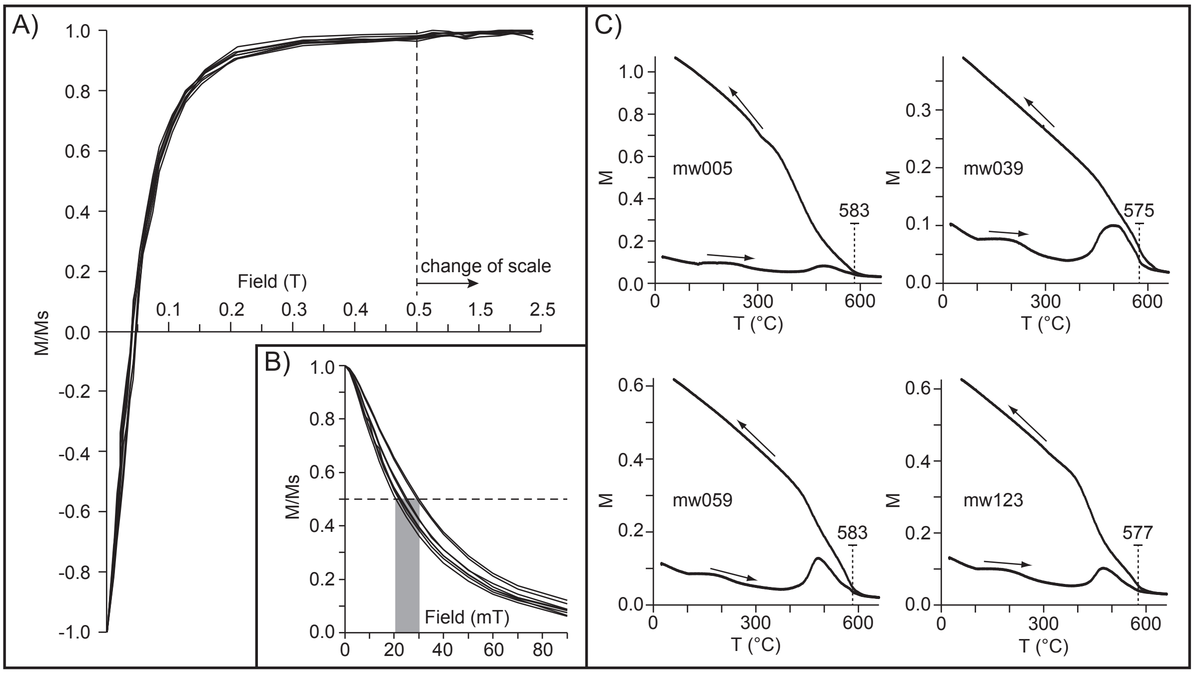
A)
M/Ms
Field (T)
change of scale
B)
M/Ms
Field (mT)
C)
mw005
583
mw039
575
mw059
583
mw123
577
M
T (°C)

Figure 2

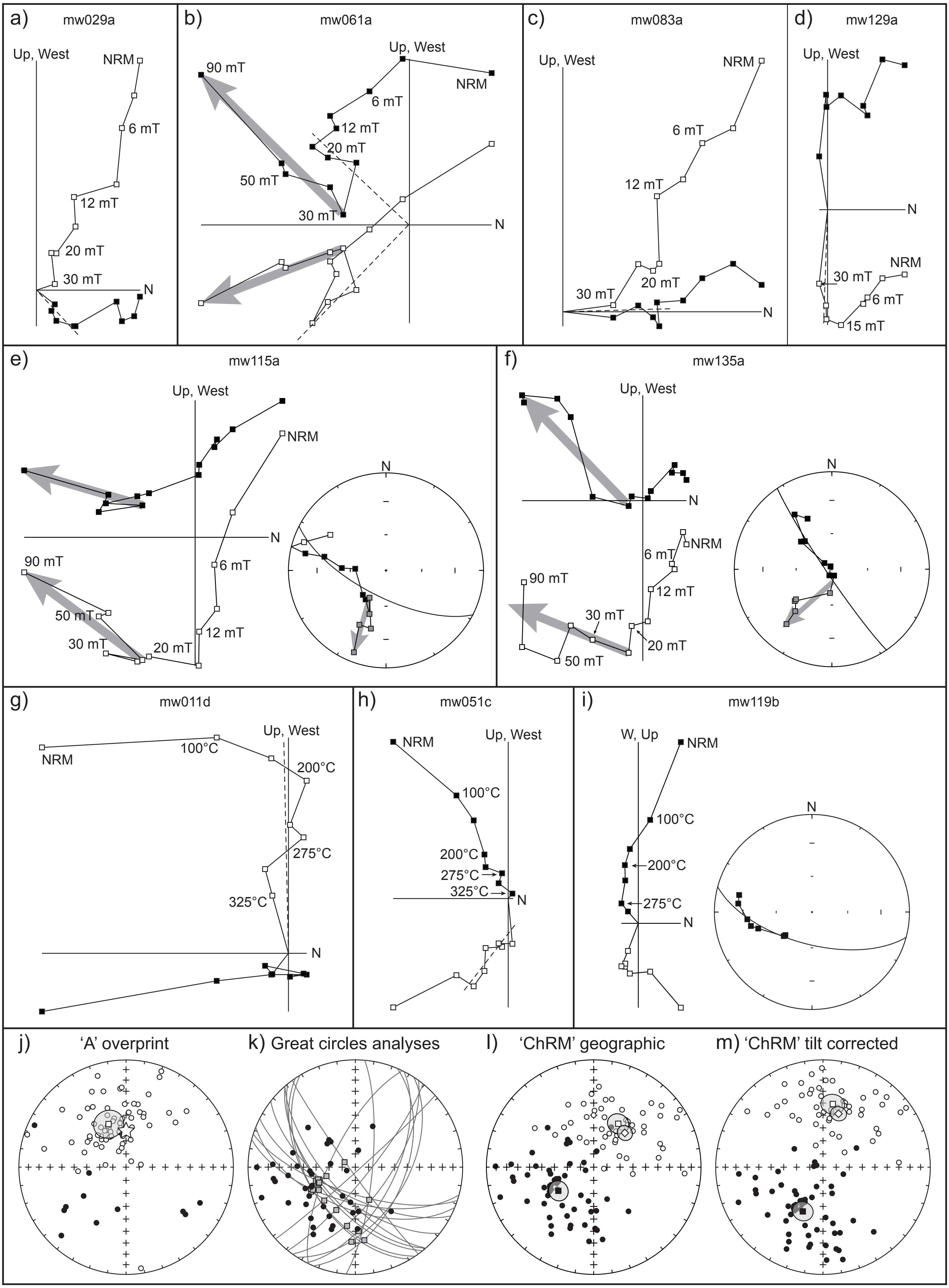
a) mw029a
Up, West
NRM
6 mT
12 mT
20 mT
30 mT
N
b) mw061a
Up, West
90 mT
NRM
6 mT
12 mT
20 mT
50 mT
30 mT
N
c) mw083a
Up, West
NRM
6 mT
12 mT
20 mT
30 mT
N
d) mw129a
Up, West
N
NRM
30 mT
6 mT
15 mT
e) mw115a
Up, West
NRM
N
90 mT
6 mT
50 mT
12 mT
30 mT
20 mT
f) mw135a
Up, West
N
6 mT
NRM
90 mT
12 mT
30 mT
20 mT
50 mT
g) mw011d
Up, West
NRM
100°C
200°C
275°C
325°C
N
h) mw051c
NRM
Up, West
100°C
200°C
275°C
325°C
N
i) mw119b
W, Up
NRM
100°C
200°C
275°C
N
j) 'A' overprint
k) Great circles analyses
l) 'ChRM' geographic
m) 'ChRM' tilt corrected

Figure 3

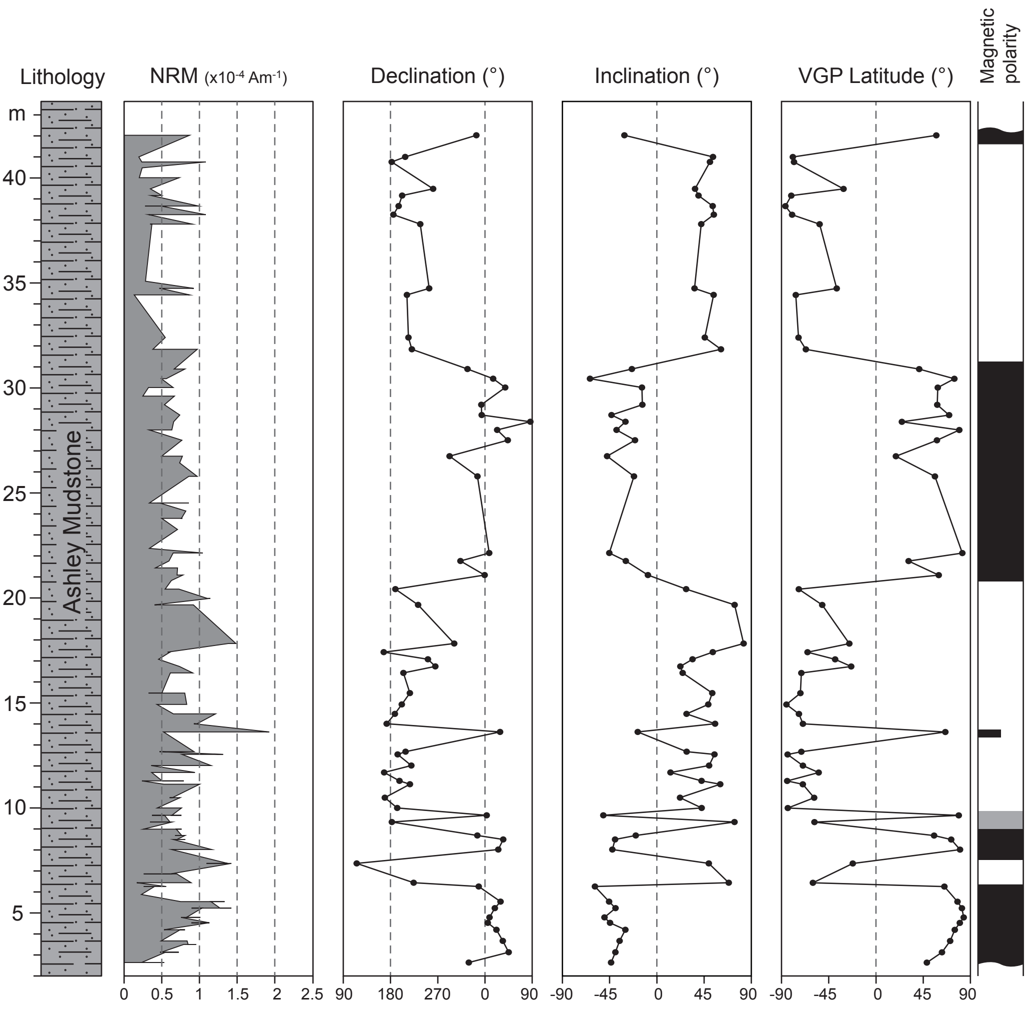
Lithology
NRM (x10-4 Am-1)
Declination (°)
Inclination (°)
VGP Latitude (°)
Magnetic polarity
m
Ashley Mudstone
40
35
30
25
20
15
10
5
0 0.5 1 1.5 2 2.5
90 180 270 0 90
-90 -45 0 45 90
-90 -45 0 45 90

Figure 4

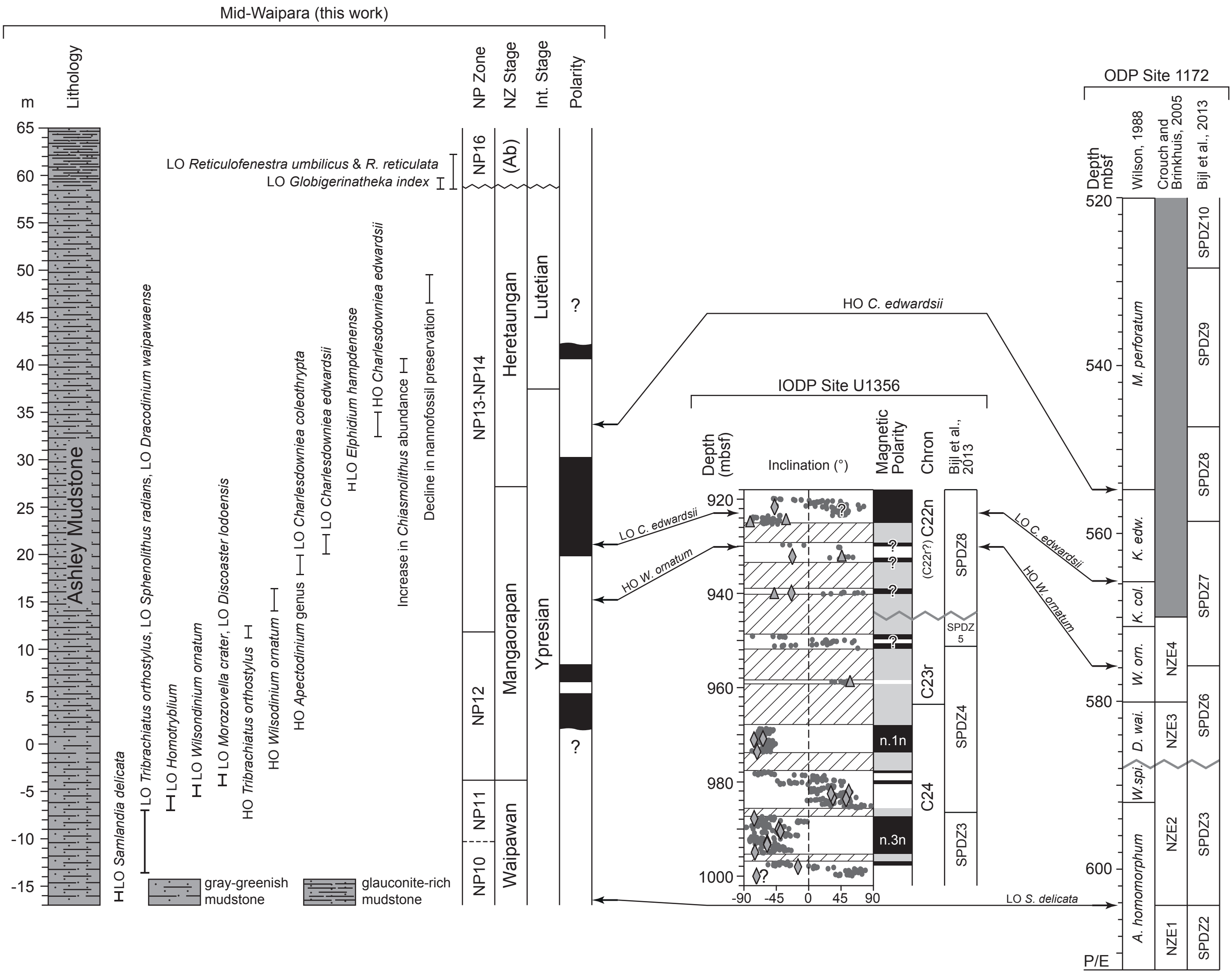
Mid-Waipara (this work)
m
Lithology
Ashley Mudstone
NP Zone
NZ Stage
Int. Stage
Polarity
NP16
NP13-NP14
NP12
NP11
NP10
(Ab)
Heretaungan
Mangaorapan
Waipawan
Lutetian
Ypresian
LO Reticulofenestra umbilicus & R. reticulata
LO Globigerinatheka index
LO Samlandia delicata
LO Tribrachiatus orthostylus, LO Sphenolithus radians, LO Dracodinium waipawaense
LO Homotryblium
LO Wilsondinium ornatum
LO Morozovella crater, LO Discoaster lodoensis
HO Tribrachiatus orthostylus
HO Wilsodinium ornatum
HO Apectodinium genus
LO Charlesdowniea coleothrypta
LO Charlesdowniea edwardsii
LO Elphidium hampdenense
HO Charlesdowniea edwardsii
Increase in Chiasmolithus abundance
Decline in nannofossil preservation
gray-greenish mudstone
glauconite-rich mudstone
HO C. edwardsii
LO C. edwardsii
HO W. ornatum
LO S. delicata
IODP Site U1356
Depth (mbsf)
Inclination (°)
Magnetic Polarity
Chron
Bijl et al., 2013
C22n
(C22r?)
C23r
C24
n.1n
n.3n
SPDZ8
SPDZ 5
SPDZ4
SPDZ3
ODP Site 1172
Depth mbsf
Wilson, 1988
Crouch and Brinkhuis, 2005
Bijl et al., 2013
M. perforatum
K. edw.
K. col.
W. orn.
D. wai.
W.spi.
A. homomorphum
NZE4
NZE3
NZE2
NZE1
SPDZ10
SPDZ9
SPDZ8
SPDZ7
SPDZ6
SPDZ3
SPDZ2
P/E

Figure 5

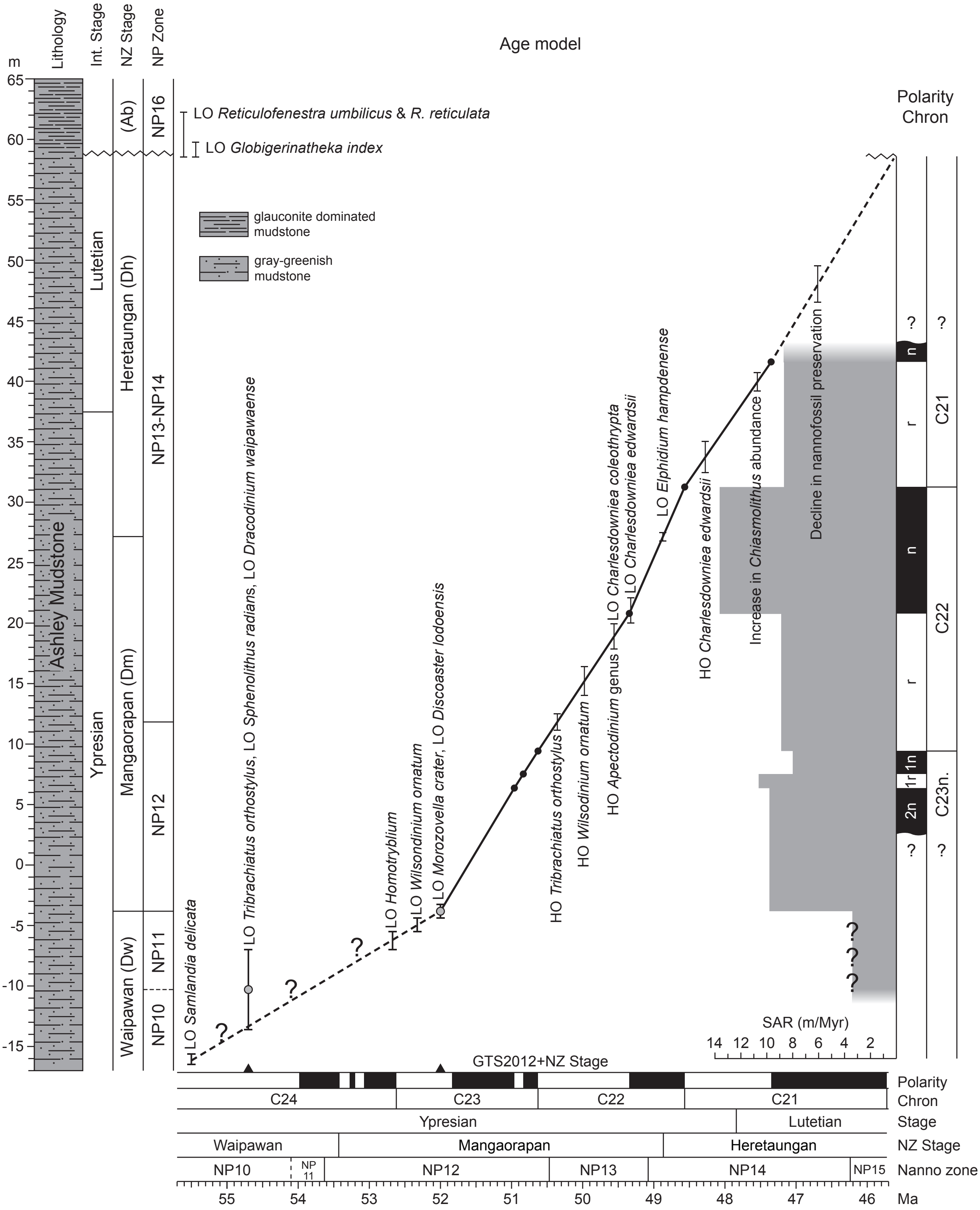

Age model
m
Lithology
Int. Stage
NZ Stage
NP Zone
Ashley Mudstone
Lutetian
Ypresian
(Ab)
Heretaungan (Dh)
Mangaorapan (Dm)
Waipawan (Dw)
NP16
NP13-NP14
NP12
NP11
NP10
glauconite dominated mudstone
gray-greenish mudstone
LO Reticulofenestra umbilicus & R. reticulata
LO Globigerinatheka index
LO Samlandia delicata
LO Tribrachiatus orthostylus, LO Sphenolithus radians, LO Dracodinium waipawaense
LO Homotryblium
LO Wilsondinium ornatum
LO Morozovella crater, LO Discoaster lodoensis
HO Tribrachiatus orthostylus
HO Wilsodinium ornatum
HO Apectodinium genus
LO Charlesdowniea coleothrypta
LO Charlesdowniea edwardsii
LO Elphidium hampdenense
HO Charlesdowniea edwardsii
Increase in Chiasmolithus abundance
Decline in nannofossil preservation
Polarity Chron
C21
C22
C23n.
SAR (m/Myr)
GTS2012+NZ Stage
C24
C23
C22
C21
Ypresian
Lutetian
Waipawan
Mangaorapan
Heretaungan
NP10
NP 11
NP12
NP13
NP14
NP15
Polarity
Chron
Stage
NZ Stage
Nanno zone
Ma

Figure 6

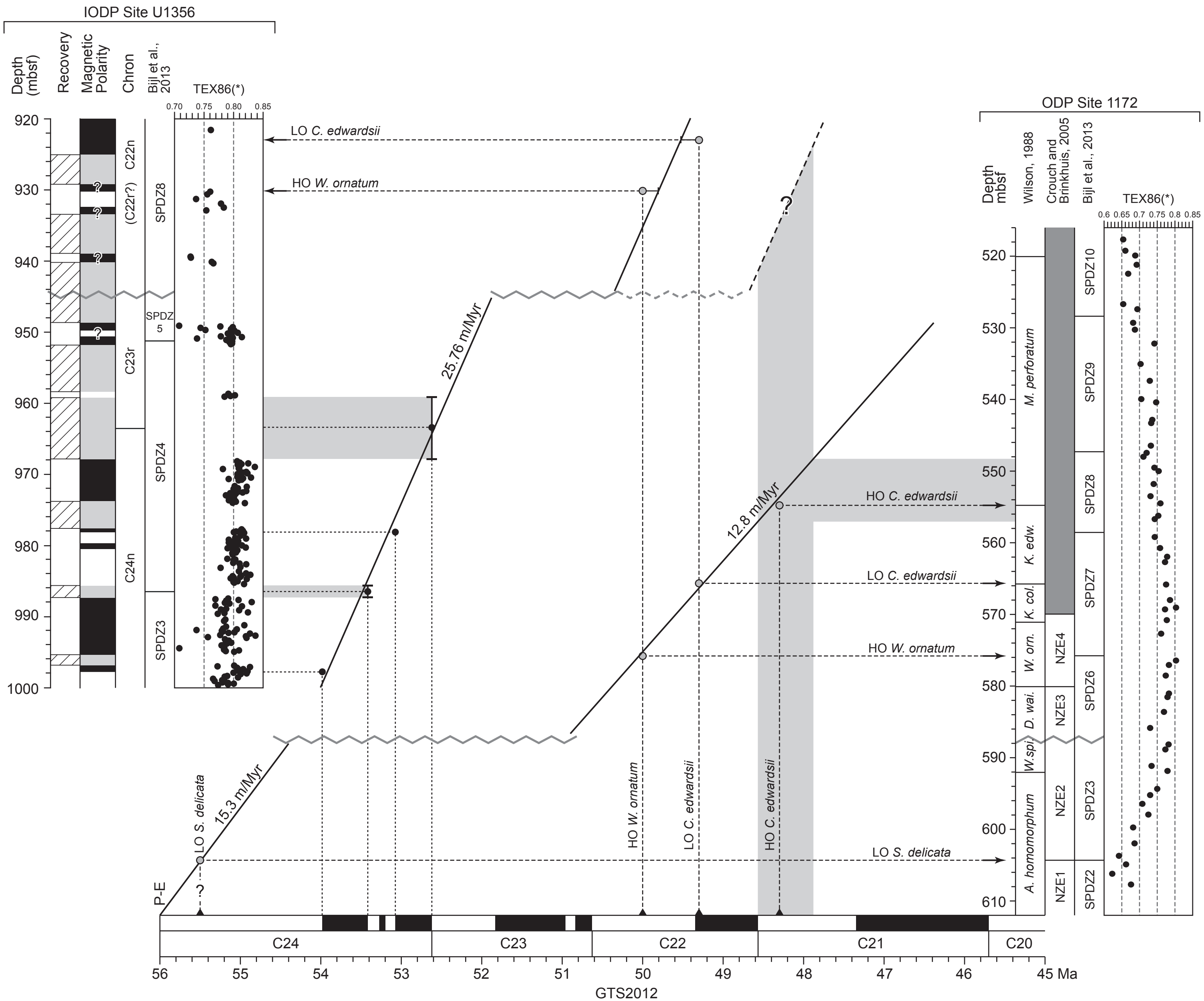

IODP Site U1356
Depth (mbsf)
Recovery
Magnetic Polarity
Chron
Bijl et al., 2013
TEX86(*)
C22n
(C22r?)
C23r
C24n
SPDZ8
SPDZ5
SPDZ4
SPDZ3
LO C. edwardsii
HO W. ornatum
25.76 m/Myr
12.8 m/Myr
15.3 m/Myr
LO S. delicata
P-E
HO C. edwardsii
ODP Site 1172
Depth mbsf
Wilson, 1988
Crouch and Brinkhuis, 2005
M. perforatum
K. edw.
K. col.
W. orn.
D. wai.
W.spi.
A. homomorphum
NZE4
NZE3
NZE2
NZE1
SPDZ10
SPDZ9
SPDZ7
SPDZ6
SPDZ2
C24
C23
C22
C21
C20
GTS2012
45 Ma

Figure 7

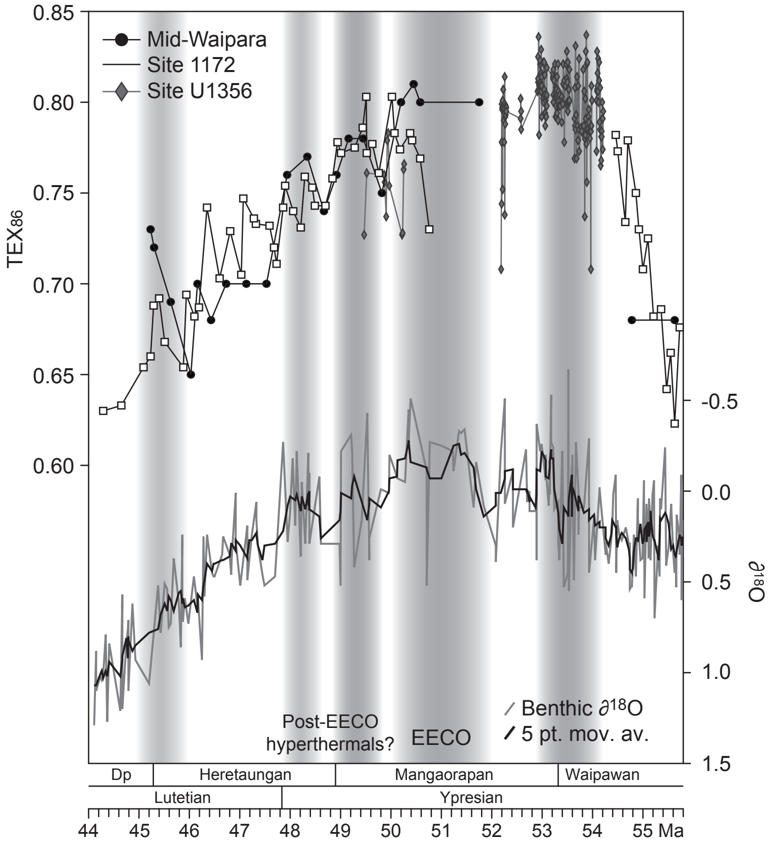
0.85
0.80
0.75
0.70
0.65
0.60
TEX86
Mid-Waipara
Site 1172
Site U1356
-0.5
0.0
0.5
1.0
1.5
∂18O
Benthic ∂18O
5 pt. mov. av.
Post-EECO
hyperthermals?
EECO
Dp
Heretaungan
Mangaorapan
Waipawan
Lutetian
Ypresian
44
45
46
47
48
49
50
51
52
53
54
55 Ma

Figure 8

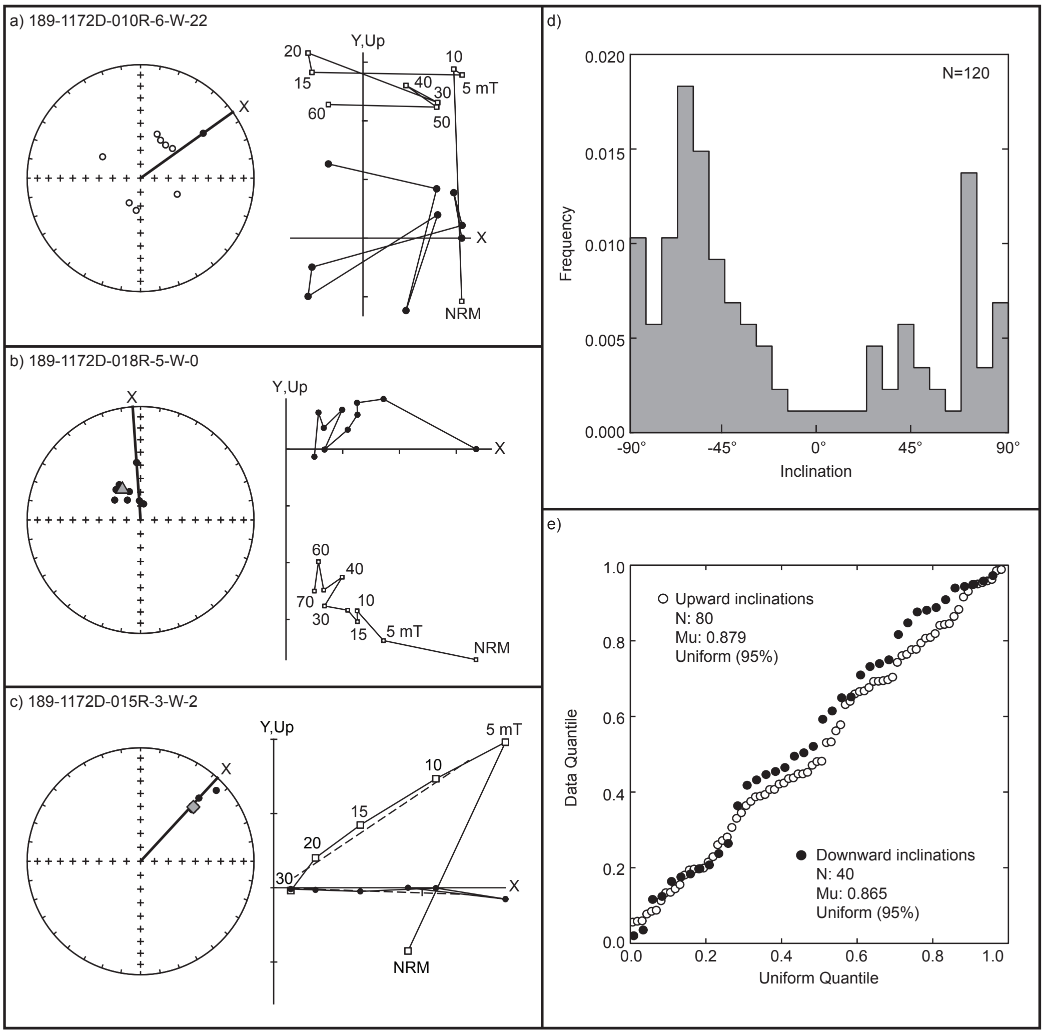

a) 189-1172D-010R-6-W-22
Y,Up
X
20
15
60
10
40
30
5 mT
50
NRM
b) 189-1172D-018R-5-W-0
Y,Up
X
60
40
70
10
30
15
5 mT
NRM
c) 189-1172D-015R-3-W-2
Y,Up
X
5 mT
10
15
20
30
NRM
d)
N=120
Frequency
0.000
0.005
0.010
0.015
0.020
-90°
-45°
0°
45°
90°
Inclination
e)
Upward inclinations
N: 80
Mu: 0.879
Uniform (95%)
Downward inclinations
N: 40
Mu: 0.865
Uniform (95%)
Data Quantile
Uniform Quantile
0.0
0.2
0.4
0.6
0.8
1.0

Figure A1

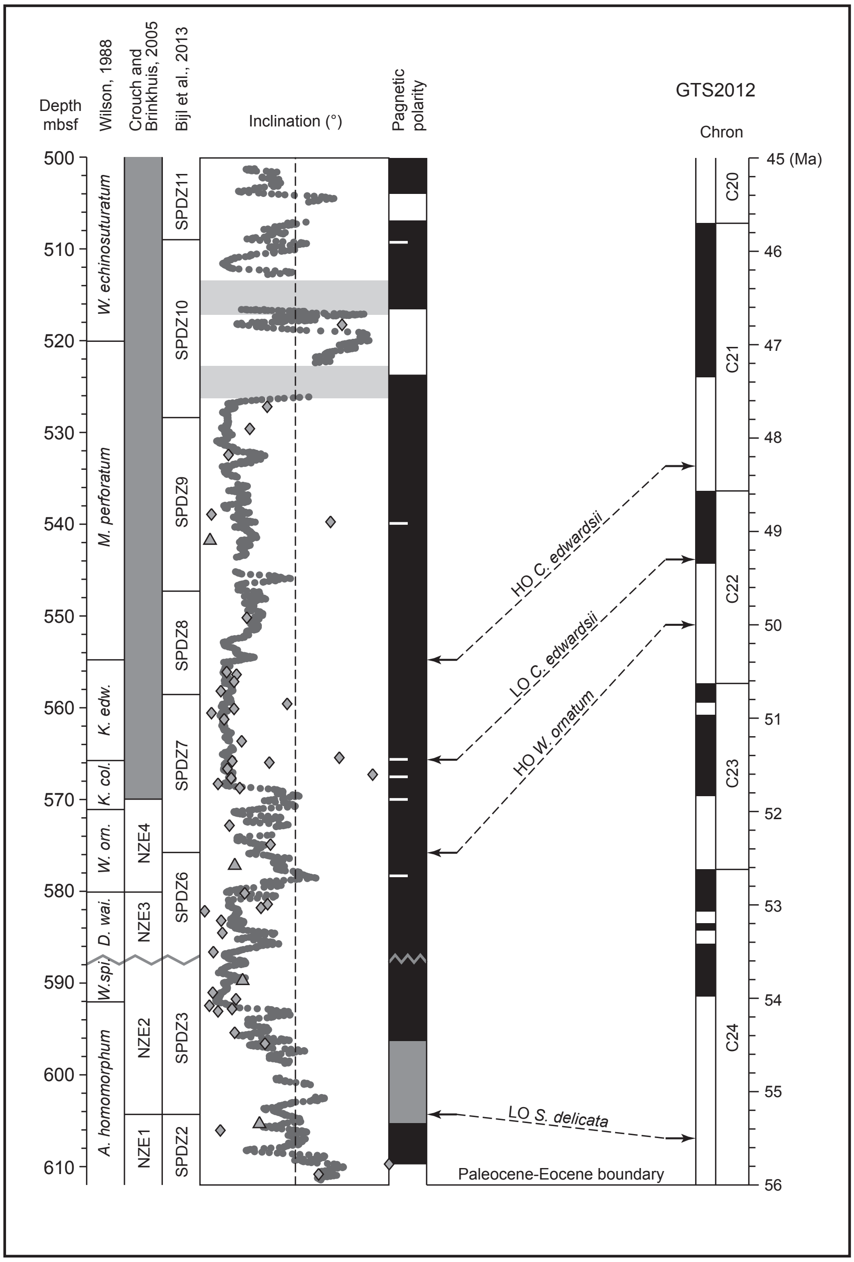
Depth mbsf
Wilson, 1988
Crouch and Brinkhuis, 2005
Bijl et al., 2013
Inclination (°)
Pagnetic polarity
GTS2012
Chron
45 (Ma)
W. echinosuturatum
M. perforatum
K. edw.
K. col.
W. orn.
D. wai.
W.spi.
A. homomorphum
NZE4
NZE3
NZE2
NZE1
SPDZ11
SPDZ10
SPDZ9
SPDZ8
SPDZ7
SPDZ6
SPDZ3
SPDZ2
C20
C21
C22
C23
C24
HO C. edwardsii
LO C. edwardsii
HO W. ornatum
LO S. delicata
Paleocene-Eocene boundary

Figure A2